Supersonic Screw Dislocations Gliding at the Shear Wave Speed

Shenyou Peng,[1,4] Yujie Wei,[1,4,*] Zhaohui Jin,[2] and Wei Yang[3]

[1]LNM, Institute of Mechanics, Chinese Academy of Sciences, Beijing 100190, China
[2]Light Alloy Net Forming National Engineering Research Center and School of Materials Science and Engineering, Shanghai Jiao Tong University, Shanghai 200240, China
[3]Institute of Applied Mechanics and Center for X-Mechanics, Zhejiang University, Hangzhou 310027, China
[4]School of Engineering Sciences, University of Chinese Academy of Sciences, Beijing 100049, China

(Received 6 October 2018; revised manuscript received 15 November 2018; published 29 January 2019)

The motion of dislocations bridges the atomistic-scale deformation events with the macroscopic strength and ductility of crystalline metals. In particular, screw dislocations, whose Burgers vector is parallel to the line, play crucial roles on plastic flow. Nevertheless, their speed limit and its stress dependence remain controversial. Using large-scale molecular dynamics simulations, we reveal that full screw dislocations and twinning partial screw-type dislocations can glide steadily at the speed of shear wave velocity. Such a scenario is excluded in existing theories due to energy dissipation singularity. We conclude that both types of screw dislocations can move supersonically. We further observe that the motion of a screw dislocation also depends on the shear stress components, which do not contribute to the resolved shear stress (RSS), in contrast to the conventional Schmid's law, which states that the motion of a dislocation is determined by the RSS.

DOI: 10.1103/PhysRevLett.122.045501

When a force exerted to a dislocation line is parallel to its slip plane and in the direction of the Burgers vector, the dislocation may glide if the resultant stress exceeds the critical resolved shear stress (RSS). The plasticity in crystalline metals depends on the collective motion of such dislocation lines [1–3], which governs the strength and ductility, as well as the dynamic behavior of crystalline materials [4–7]. What is unique to dislocation motion is the acoustic wave propagations of the elastic media where dislocations reside. When dislocations move supersonically—namely, at a velocity greater than the shear wave velocity for screw dislocations and greater than the longitudinal wave velocity if the dislocations are of pure edge type—they radiate sound waves and intake singular energy dissipation based on general elasticity theory [8]. Mathematically, a singular radiation-free state does exist for edge dislocations gliding supersonically in isotropic solids [9]. Further analysis predicted the existence of supersonic dislocations [9–14]. It is noted that a smeared-out treatment [10,12–14] to dislocation reduces the stress singularity, but it brings in additional parameters to describe the infinitesimal dislocation distribution. That leads to the long-standing debate on the speed limits of dislocations.

In contrast to the theoretical analysis, modeling the physical state of dislocation motion using faithful atomic interaction may circumvent the limitation of elasticity theory and shed light on the kinetics of dislocations [15–18]. Gumbsch and Gao [19] first showed stable edge dislocations with transonic and supersonic velocities in their computational study. Combined with other reports [20–23], it was found that, under sufficiently high RSS, an edge dislocation can break the shear wave barrier and move faster than the longitudinal wave velocity, supported by recent experiments [24,25]. Such high speed dislocations can introduce deformation transition from dislocation motion to deformation twinning in conventional high stacking fault metals [6]. Most studies, however, dealt with edge dislocations and those on screw ones are rarely seen. It is believed that a screw dislocation will suffer instability when its traveling speed approaches the shear wave speed [18,26]. The difficulty to observe supersonic screw dislocations in both experiments and simulations casts doubt on the theory predicting the existence of supersonic screw dislocations. Because of their overwhelming contribution to the plasticity in crystalline materials, the kinetics of screw dislocations is crucial to the dynamic response of materials [4].

A detailed description about the simulation is supplied in the Supplemental Material Note 1 [27]. A dipole of perfect screw dislocations (SDs) is generated by a procedure illustrated in Fig. 1(a). Given the significance of twinning partials in deformation twinning [34,35], we also explore the dynamics of a Twinning screw partial dislocation (TSPD) residing in twin boundaries. Atomic structures of SDs and TSPDs are shown in Fig. S1 [27]. After relaxation, a perfect SD splits into two Shockley partials bounded by a stacking fault (SF) in between, following the reaction $(a/2)[1\bar{1}0] = (a/6)[1\bar{2}1] + (a/6)[2\bar{1}\,\bar{1}] + \mathrm{SF}$ (see Supplemental Material Note 2 and Fig. S2a [27]). Note that the Burgers vector of the TSPD is the same as the

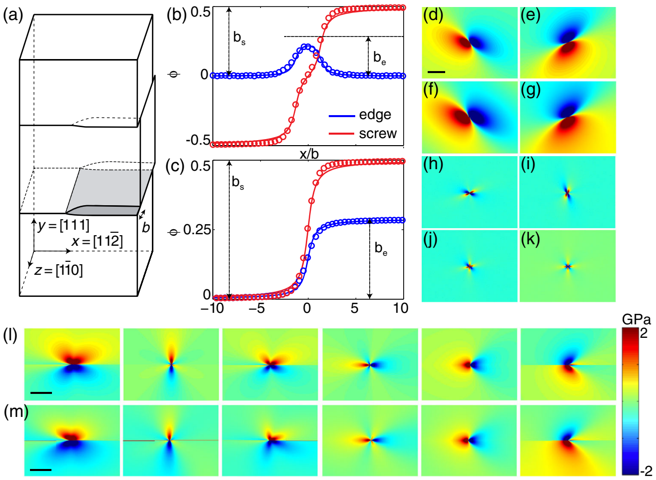

FIG. 1. Structures and stress fields of perfect screw dislocations and twinning screw partial dislocations. (a) Illustration of the generation of a SD dipole and the coordinates defined by the crystallographic orientations $x = [11\bar{2}]$, $y = [111]$, $z = [1\bar{1}0]$. (b), (c) Normalized displacement shift ϕ between the gliding plane and the glided plane nearby the dislocation core (b) for the SD and (c) for the TSPD. Here b_e and b_s are the magnitude of the edge and screw part of the Burgers vector. The theory (solid lines) matches well with simulations (circles). (d)–(k) Stress fields of the full screw dislocation: σ_{yz} from theoretical prediction (d) and simulation (f); σ_{xz} from theoretical prediction (e) and simulation (g); Other four stress components $\sigma_{xx}, \sigma_{yy}, \sigma_{zz}$, and σ_{xy} from simulation are shown in (h)-(k). (l) The respective stress fields $\sigma_{xx}, \sigma_{yy}, \sigma_{zz}, \sigma_{xy}, \sigma_{yz}$, and σ_{xz} of the TSPD from theoretical prediction and (m) MD simulations. (Scale bar = 15 nm.)

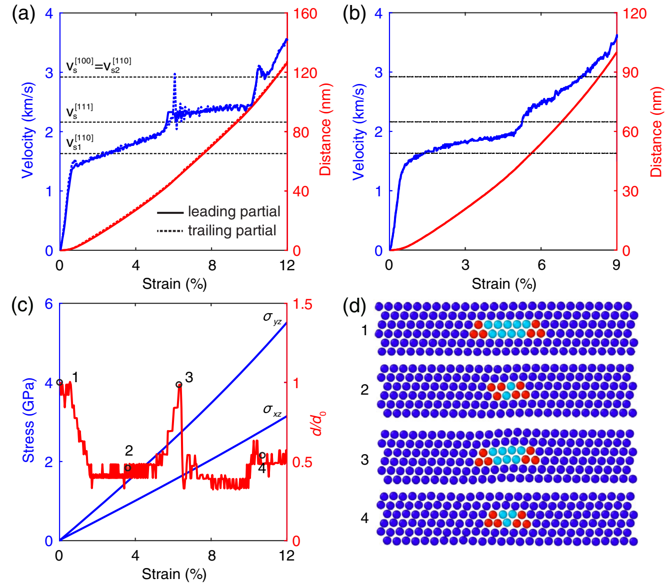

FIG. 2. Motion of screw dislocations under shear straining. (a) Travel distance vs strain (red) and velocity vs strain (blue) of the SD. (b) Motion of a TSPD. Here $v_{s1}^{[110]} = 1.63$, $v_s^{[111]} = 2.16$, and $v_s^{[100]} = v_{s2}^{[110]} = 2.92$ km/s are three shear wave speeds in single crystal copper. (c) Stacking fault width d (red) of the SD and the stress-strain relation (blue) as a function of straining, where d_0 is the stacking fault width at a stress-free state. (d) Snapshots of stacking fault width corresponding to points keyed in (c), and atoms are colored by the common neighbor analysis method.

dissociated SD but stacking fault free. The displacement mismatch between the neighboring intact layer and the dislocated layer characterizes the core structure of the dissociated SD and the TSPD, as seen in Figs. 1(b) and 1(c). The dislocation core can also be featured by the misfit density, as Fig. S2 [27] shows. Detailed atomistic structures of the dislocations before and after relaxation are illustrated in Fig. S3 [27].

We adopted the classical anisotropic elasticity theory of straight dislocations to capture the stress field of screw dislocations (see Supplemental Material Note 3 [27]). In Figs. 1(d) and 1(e) we demonstrate the theoretical predictions of stress components σ_{yz}, σ_{xz}, respectively, where we ignored the dissociation for simplicity, as the dissociated edge part only induces short-range stress fields [see Figs. 1(h)–1(k)]. As a comparison, the stress fields σ_{yz}, σ_{xz} from direct MD simulations are plotted in Figs. 1(f) and 1(g), respectively. The other four stress components $\sigma_{xx}, \sigma_{yy}, \sigma_{zz}, \sigma_{xy}$ introduced by a SD are shown in Figs. 1(h)–1(k); those stress components are secondary and their magnitude decreases progressively with the distance to the dislocation core. The static stress fields from theoretical prediction and MD simulations shown in Fig. 1 demonstrate the accuracy of the atomistic interaction.

In contrast, the stress from the edge part becomes significant in TSPD, and we show the six stress fields of the TSPD from theory and MD simulations in Figs. 1(l) and 1(m). The presence of the twin boundaries make those stress fields change dramatically. In contrast to the negligible medium- to long-range stress fields, i.e., σ_{xx}, $\sigma_{yy}, \sigma_{zz}, \sigma_{xy}$ for a perfect SD, those introduced by the TSPD are nonlocal. This behavior may subsequently influence the activities of deformation twinning accommodated by such twinning partials.

We apply a shear deformation ε_{yz} to the simulation box, which drives the dislocation to glide along the x direction. Figures 2(a) and 2(b) show travel distance and velocity curves for both types of dislocations during shearing. For the SD, the curves of the leading and the trailing partials are plotted separately. As a reference, we have calculated the three shear wave speeds in Cu by solving the wave equation in anisotropic elastic media (see Supplemental Material Note 4 [27]) and obtained $v_{s1}^{[110]} = 1.63$, $v_s^{[111]} = 2.16$, and $v_s^{[100]} = v_{s2}^{[110]} = 2.92$ km/s.

From Fig. 2(a), we see that the SD first accelerates in response to the rising of shear strain. When its velocity reaches $v_{s1}^{[110]}$, the acceleration drops while the velocity continues to increase toward the second shear wave speed $v_s^{[111]}$, followed by a velocity jump. Then the dislocation

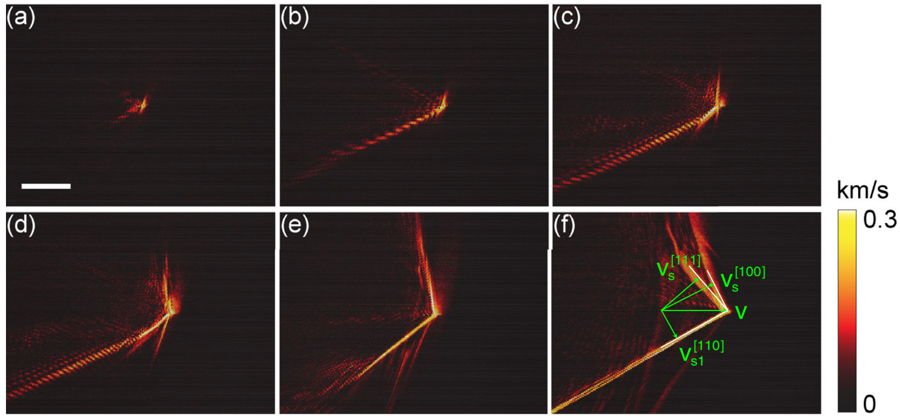

FIG. 3. MD snapshots of the SD at different velocities. (a) Fast acceleration at $v = 0.8$ km/s. (b) Slow acceleration at $v = 1.8$ km/s. (c), (d) The first velocity jump across the shear wave speed $v_s^{[111]}$: (c) trailing partial glides slower than leading partial, (d) trailing partial catches up with the leading partial. (e) Steady motion at $v = 2.36$ km/s, which is faster than $v_s^{[111]}$. (f) Supersonic motion with $v = 3.1$ km/s, where a shock wave induced by the dislocation is clearly seen. The corresponding shear wave velocity of each Mach cone is marked. (Scale bar = 8 nm.)

moves steadily at a speed slightly above $v_s^{[111]}$. Further straining can drive both partials of the SD moving faster than the third shear wave speed $v_s^{[100]}$, i.e., supersonically. At $\varepsilon_{yz} \geq 12\%$, massive nucleated dislocations appears in the sample. As seen from the stress-strain curve in Fig. 2(c), the applied shear strain ε_{yz} induces two shear stress components σ_{yz} and σ_{xz} due to elastic anisotropy. The travel distance (red) and velocity (blue) curves of the TSPD residing in a twin boundary, as seen in Fig. 2(b), demonstrate that TSPD can also move beyond the "limiting" supersonic wave speed (see Supplemental Material Note 5 and Fig. S5 [27]), regardless of the significant difference in stress fields between the SD and TSPD (see Fig. 1). It is emphasized that the stress levels when the dislocation reaches the shear wave velocities are below the material's ideal strength, as seen in Fig. S4 [27].

The leading partial and the trailing partial of the SD behave distinctly after shearing. That causes the variation of the stacking fault width d, as detailed in Figs. 2(c) and 2(d). Both the equilibrium shape and width d_0 can be well captured by Eqs. (S1) and (S2) [27]. In the accelerating region, the velocities of both partials increase continuously but the SF may change substantially. It can shrink till there is only one layer of atoms between two partials ($d \sim 6$ Å), as seen in points 1 and 2 in Fig. 2(c). When the velocity reaches the shear wave speed $v_s^{[111]}$ at ~6% strain, d increases suddenly as the dislocation passes the second shear wave speed, as shown at point 3 in Fig. 2(c), and then decreases again, shown at point 4 in Fig. 2(c), which is consistent with the previous observation [26]. It is noted that, not only is the SF width a function of the velocity, but also the dislocation core width depends on the dislocation velocity; the change of the latter is rather small and so the corresponding information is not shown. In Figs. 3(a)–3(f), we show the velocity field v induced by the moving SD at different speeds. When the dislocation moves supersonically, a Mach cone is clearly generated [Fig. 3(f)].

Based on the continuum mechanics prediction, a singular energy dissipation would be required to sustain a dislocation moving at the shear wave speed. We examine the validity of this continuum prediction. We first apply shear to the samples at the strain rate of 2×10^9/s until the velocity of the SD reaches the shear wave speed of $v_s^{[100]}$. We then maintain the shearing load constant to see whether the velocity of the dislocation is stable. As seen in Fig. 4 for the SD, dislocations can move steadily at $v_s^{[100]}$. To check the robustness of the results, we performed three calculations for each type of dislocation by keeping its velocity at three scenarios: slightly slower than $v_s^{[100]}$, equal to $v_s^{[100]}$, and slightly faster than $v_s^{[100]}$. The exact values are keyed in Fig. 4(a), and the respective atomic velocity contours of the SD are shown in Figs. 4(b)–4(d). The relation between the velocities is obtained from the Mach cone. Those results indicate that a SD can move steadily at the shear wave speed, which breaks the conventional conclusion from continuum elastic theory. This discrepancy may originate from the fact that the atomic structure of a dislocation core is discrete in nature where there is no singularity, in contrast to that assumed in continuum. Consequently, the barrier energy for a dislocation that moves at the shear wave speed $v_s^{[100]}$ is finite and attainable. As a comparison, we also explore the motion of the TSPD at the shear wave speed. As seen in Fig. S6 [27], the TSPD can move steadily at the shear wave velocity as well.

When applying a shear strain ε_{yz}, we induce two shear stress components, σ_{yz} and σ_{xz}, due to elastic anisotropy [Fig. 2(c)]. Although σ_{xz} does not contribute to the RSS as predicted by Schmid's law [36], which is a foundation of

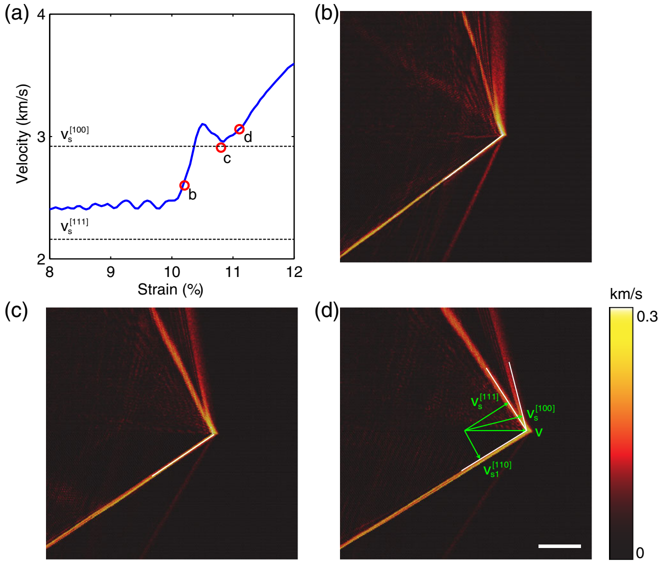

FIG. 4. A SD moves at the shear wave speed $v_s^{[100]}$. (a) The blue line is the amplified velocity-strain curve from Fig. 2(a). Three red circles mark the velocities at which the dislocation could glide steadily. (b)–(d) Velocity fields v induced by steadily moving dislocation at the three velocities keyed in (a), respectively. (Scale bar = 8 nm.)

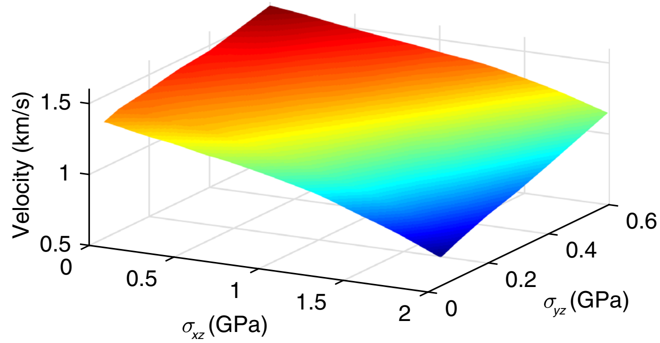

FIG. 5. Non-Schmid effect for a SD in FCC Cu. Shear stress σ_{yz} contributes to the resolved shear stress τ_{RSS} and dominates the dislocation motion according to Schmid's law. One observes here that σ_{xz} also bears a non-negligible effect on dislocation mobility even though it does not contribute to τ_{RSS}.

plasticity theories in dislocation dominated mechanisms [3,37,38]; it also alters the dislocation motion. For three-dimensional stress states, the resolved shear stress τ_{RSS} is calculated as $\tau_{\mathrm{RSS}} = \boldsymbol{m}\cdot(\boldsymbol{\sigma}\cdot\boldsymbol{n})$, where $\boldsymbol{n} = (0,1,0)$ is the slip plane normal and $\boldsymbol{m} = (0,0,1)$ is the direction of the dislocation's Burgers vector. Using Schmid's law, we see that only σ_{yz} contributes to τ_{RSS} for the screw dislocations in Fig. 1(a), implying that this stress component is responsible for the motion of dislocations in the prescribed slip system.

To identify whether the stress components σ_{xz} also alters the dislocation motion, a quasi-*NPT* ensemble is employed. We first increase σ_{yz} and then keep σ_{yz} at a constant value so that the dislocation moves at a velocity $v < v_{s1}^{[110]}$. After a transient stage, the dislocation glides steadily at a constant velocity. We then apply σ_{xz} from 0 to 2 GPa and see how it may change the dislocation speed. By simulating different σ_{yz} (from 50 to about 600 MPa), we construct in Fig. 5 the dislocation velocity profile at different combinations of σ_{yz} and σ_{xz}. Although σ_{xz} does not contribute to the resolved shear stress, its influence on the dislocation mobility is considerable. This is clear evidence of the non-Schmid behavior of the dislocation.

As proposed by Qin and Bassani [39], the generalized stress measure τ^* in a particular slip system is linearly combined by the resolve shear stress and the non-Schmid stresses as $\tau^* = \tau_{\mathrm{RSS}} + \sum_i a_i\tau_i$, where τ_i are the non-Schmid stress components and a_i are their weighting coefficients. We examine the physical mechanism behind the non-Schmid effect in an anisotropic crystal with our simulation results. In the coordinate given in Fig. 1(a), we have the following shear stress and shear strain relationship:

$$\begin{bmatrix}\sigma_{yz}\\ \sigma_{xz}\end{bmatrix} = \begin{bmatrix}\frac{1}{3}(C_{11}-C_{12}+C_{44}) & \frac{\sqrt{2}}{6}(C_{12}-C_{11}+2C_{44})\\ \frac{\sqrt{2}}{6}(C_{12}-C_{11}+2C_{44}) & \frac{1}{6}(C_{11}-C_{12}+4C_{44})\end{bmatrix} \times \begin{bmatrix}\varepsilon_{yz}\\ \varepsilon_{xz}\end{bmatrix}. \quad (1)$$

As the deformation along the dislocation line is negligible, we have $(\partial/\partial z) = 0$; hence, $\varepsilon_{yz} = (\partial u_z/\partial y)$, $\varepsilon_{xz} = (\partial u_z/\partial x)$. The inverse of Eq. (1) is written as

$$\begin{bmatrix}\frac{\partial u_z}{\partial y}\\ \frac{\partial u_z}{\partial x}\end{bmatrix} = \begin{bmatrix}S_{55} & S_{56}\\ S_{56} & S_{66}\end{bmatrix}\begin{bmatrix}\sigma_{yz}\\ \sigma_{xz}\end{bmatrix},$$

$$\begin{bmatrix}S_{55} & S_{56}\\ S_{56} & S_{66}\end{bmatrix} = \frac{2}{3(C_{11}-C_{12})}\begin{bmatrix}A+2 & \sqrt{2}(A-1)\\ \sqrt{2}(A-1) & 2A+1\end{bmatrix}, \quad (2)$$

where S_{ij} are the components in the compliance tensor $\boldsymbol{S} = \boldsymbol{C}^{-1}$. The anisotropic parameter A is defined as $A = [(C_{11}-C_{12})/2C_{44}]$ and $A = 1$ for isotropic solids. For the screw dislocation, the strain $\partial u_z/\partial y$ dominates dislocation motion as it supplies the regular driving force τ^*, which is proportional to $\partial u_z/\partial y$; meanwhile, $\partial u_z/\partial x$ contributes to the driving force τ_{cs} for the tendency of cross slip. The relationship of both stress components with the applied stress could be determined from Eq. (2), i.e., $\tau^* \propto (\partial u_z/\partial y) = S_{55}\sigma_{yz} + S_{56}\sigma_{xz}$ and $\tau_{\mathrm{cs}} \propto (\partial u_z/\partial x) = S_{56}\sigma_{yz} + S_{66}\sigma_{xz}$. We then obtain the effective resolved shear stress as

$$\tau^* = \sigma_{yz} + \frac{S_{56}}{S_{55}}\sigma_{xz}. \quad (3)$$

This relationship is obtained with the consistent condition that $\tau^* = \sigma_{yz}$ if $A = 1$. We focus on demonstrating the nonzero component in Eqs. (1)–(3) for screw dislocation motion as other stress components $\sigma_{xx}, \sigma_{yy}, \sigma_{zz}, \sigma_{xy}$ have negligible influence on screw dislocation motion. The component σ_{xy} does change the stacking fault width as it influences the motion of the edge part in the MD simulations, since all complete screw dislocations will decompose into two partials with a stacking fault in between. Equation (3) reflects the nature of the non-Schmid effect in anisotropic crystals. For Cu, we yield $\tau^* = \sigma_{yz} - 0.42\sigma_{xz}$. It is suggested that Eq. (3) should be used to replace the broadly used definition to calculate the RSS of Cu in current crystal plasticity models, where the accuracy of the Schmid law is taken for granted.

To summarize, we reveal that a screw dislocation can move supersonically. We find that screw dislocations can glide steadily at the shear wave speed, and this observation overthrows the long-standing conventional theory that the energy dissipation for a screw dislocation moving at the shear wave speed becomes infinite, and is hence impossible. It is found that the stress component that does not contribute to the RSS affects the dislocation motion dramatically. The findings reported here address the long-standing debate whether a SD can glide steadily at the shear wave speed or even supersonically and pave the way of better understanding to the dynamic behavior of crystalline materials [40].

S. P. and Y. W. acknowledge support from the National Natural Science Foundation of China (Grants No. 11425211 and No. 11790291) and the Strategic Priority Research Program of the Chinese Academy of Sciences (XDB22020200). The simulations were conducted at the Supercomputing Center of CAS.

*Corresponding author.
yujie_wei@lnm.imech.ac.cn

[1] G. I. Taylor, Proc. R. Soc. A **145**, 362 (1934).
[2] E. Orowan, Z. Phys. **89**, 605 (1934).
[3] A. S. Argon, *Strengthening Mechanisms in Crystal Plasticity* (Oxford University Press, Oxford, 2007).
[4] M. A. Meyer, *Dynamic Behavior of Materials* (John Wiley & Sons Inc., Hoboken, NJ, 1994).
[5] T. Zhu, J. Li, A. Samanta, H. G. Kim, and S. Suresh, Proc. Natl. Acad. Sci. U.S.A. **104**, 3031 (2007).
[6] F. Zhao, L. Wang, D. Fan, B. X. Bie, X. M. Zhou, T. Suo, Y. L. Li, M. W. Chen, C. L. Liu, M. L. Qi, M. H. Zhu, and S. N. Luo, Phys. Rev. Lett. **116**, 075501 (2016).
[7] K. Lu, Nat. Rev. Mater. **1**, 16019 (2016).
[8] P. M. Anderson, J. P. Hirth, and J. Lothe, *Theory of Dislocations*, 3rd ed. (Cambridge University Press, Cambridge, England, 2017).
[9] J. D. Eshelby, Proc. Phys. Soc. London Sect. B **69**, 1013 (1956).
[10] J. Weertman and J. R. Weertman, Moving dislocations, in *Dislocations in Solids*, edited by F. R. N. Nabarro (North-Holland Publishing Company, Oxford, 1980).
[11] P. Rosakis, Phys. Rev. Lett. **86**, 95 (2001).
[12] X. Markenscoff and S. R. Huang, J. Mech. Phys. Solids **56**, 2225 (2008).
[13] X. Markenscoff and S. R. Huang, Appl. Phys. Lett. **94**,021906 (2009).
[14] M. Lazar, Proc. R. Soc. A **465**, 2505 (2009).
[15] S. J. Zhou, D. L. Preston, P. S. Lomdahl, and D. M. Beazley, Science **279**, 1525 (1998).
[16] H. Koizumi, H. O. K. Kirchner, and T. Suzuki, Mater. Sci. Eng. A **309–310**, 117 (2001).
[17] J. Marian, W. Cai, and V. V. Bulatov, Nat. Mater. **3**, 158 (2004).
[18] D. Mordehai, I. Kelson, and G. Makov, Phys. Rev. B **74**, 184115 (2006).
[19] P. Gumbsch and H. Gao, Science **283**, 965 (1999).
[20] D. L. Olmsted, L. G. Hector, Jr., W. A. Curtin, and R. J. Clifton, Model. Simul. Mater. Sci. Eng. **13**, 371 (2005).
[21] Z. H. Jin, H. J. Gao, and P. Gumbsch, Phys. Rev. B **77**, 094303 (2008).
[22] H. Tsuzuki, P. S. Branicio, and J. P. Rino, Acta Mater. **57**, 1843 (2009).
[23] Y. J. Wei and S. Y. Peng, Sci. China Phys. Mech. Astron. **60**, 114611 (2017).
[24] V. Nosenko, S. Zhdanov, and G. Morfill, Phys. Rev. Lett. **99**, 025002 (2007).
[25] V. Nosenko, G. E. Morfill, and P. Rosakis, Phys. Rev. Lett. **106**, 155002 (2011).
[26] Z. Q. Wang and I. J. Beyerlein, Phys. Rev. B **77**, 184112 (2008).
[27] See Supplemental Material at http://link.aps.org/supplemental/10.1103/PhysRevLett.122.045501 for more modeling details, which includes Refs. [8,28–33].
[28] S. Plimpton, J. Comput. Phys. **117**, 1 (1995).
[29] Y. Mishin, M. J. Mehl, D. A. Papaconstantopoulos, A. F. Voter, and J. D. Kress, Phys. Rev. B **63**, 224106 (2001).
[30] D. Faken and H. Jónsson, Comput. Mater. Sci. **2**, 279 (1994).
[31] R. Peierls, Proc. Phys. Soc. London **52**, 34 (1940).
[32] J. D. Eshelby, W. T. Read, and W. Shockley, Acta Metall. **1**, 251 (1953).
[33] C. Kittel, *Introduction to Solid State Physics* (Wiley, Hoboken, 2005), 8th ed.
[34] Q. S. Pan, H. F. Zhou, Q. H. Lu, H. J. Gao, and L. Lu, Nature (London) **551**, 214 (2017).
[35] X. Y. Li, Y. J. Wei, L. Lu, K. Lu, and H. J. Gao, Nature (London) **464**, 877 (2010).
[36] E. Schmid and W. Boas, Kristallplastizität, *Struktur und eigenschaften der materie eine monographiensammlung, XVII* (Springer, Berlin, 1935).
[37] R. Hill and J. R. Rice, J. Mech. Phys. Solids **20**, 401 (1972).
[38] R. J. Asaro and A. Needleman, Acta Metall. **33**, 923 (1985).
[39] Q. Qin and J. L. Bassani, J. Mech. Phys. Solids **40**, 813 (1992).
[40] B. Devincre, T. Hoc, and L. Kubin, Science **320**, 1745 (2008).